ENVIRONMENTAL RESEARCH
LETTERS

LETTER • OPEN ACCESS

Long-wave infrared identification of smoldering peat fires in Indonesia with nighttime Landsat data

To cite this article: Christopher D Elvidge *et al* 2015 *Environ. Res. Lett.* **10** 065002

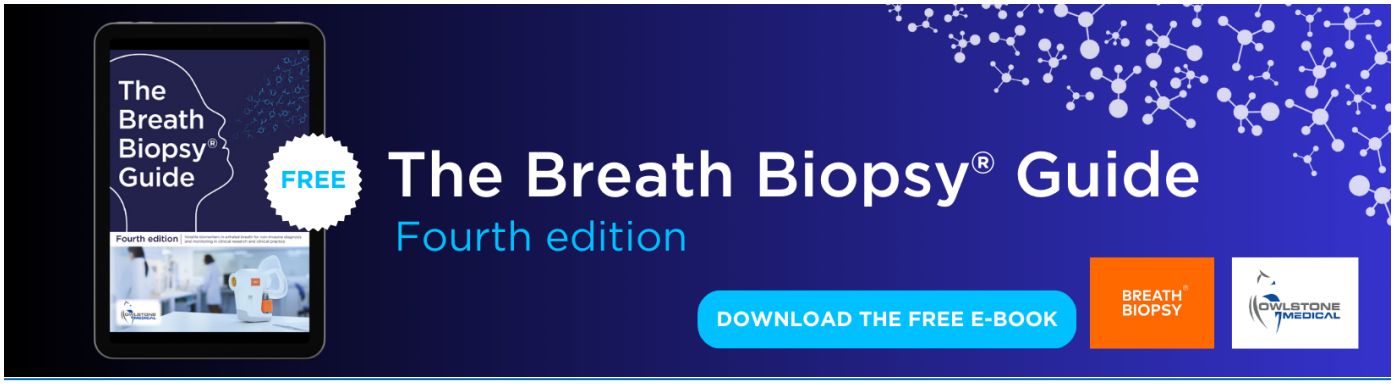

Environmental Research Letters

LETTER

Long-wave infrared identification of smoldering peat fires in Indonesia with nighttime Landsat data

Christopher D Elvidge[1], **Mikhail Zhizhin**[2,3], **Feng-Chi Hsu**[2], **Kimberly Baugh**[2], **M Rokhis Khomarudin**[4], **Yenni Vetrita**[4], **Parwati Sofan**[4], **Suwarsono**[4] **and Dadang Hilman**[5]

[1] Earth Observation Group, NOAA National Geophysical Data Center, 325 Broadway, Boulder, Colorado 80305, USA
[2] Cooperative Institute for Research in the Environmental Sciences, University of Colorado, Boulder, Colorado, USA
[3] Space Research Institute, Russian Academy of Sciences, Moscow, Russia
[4] National Institute of Aeronautics and Space (LAPAN), Jakarta, Indonesia
[5] Indonesia Climate Change Center, Jakarta, Indonesia

E-mail: chris.elvidge@noaa.gov

Keywords: Landsat, fire detection, peat fire, smoldering, flaming, Indonesia

OPEN ACCESS

RECEIVED
14 December 2014

REVISED
31 March 2015

ACCEPTED FOR PUBLICATION
2 April 2015

PUBLISHED
2 June 2015

Abstract

Smoldering peat fires in Indonesia are responsible for large quantities of trace gas and particulate emissions. However, to date no satellite remote sensing technique has been demonstrated for the identification of smoldering peat fires. Fires have two distinct combustion phases: a high temperature flaming and low temperature smoldering phases. The flaming phase temperature is approximately twice that of the smoldering phase. This temperature differential results in a spectral displacement of the primary radiant emissions of the two combustion phases. It it is possible to exploit this spectral displacement using widely separated wavelength ranges. This paper examines active fire features found in short-wave infrared (SWIR) and long-wave infrared (LWIR) nighttime Landsat data collected on peatlands in Sumatra and Kalimantan. Landsat 8's SWIR bands are on the leading edge of flaming phase radiant emissions, with only minor contribution from the smoldering phase. Conversely, Landsat 8's LWIR bands are on the trailing edge of smoldering phase radiant emissions. After examining the LWIR fire features, we conclude that they are the result of smoldering phase combustion. This has been confirmed with field validation. Detection limits for smoldering peat fires in Landsat 8 is in the 40–90 m^2 range. These results could lead to improved management of peatland fires and emission modeling.

1. Introduction

There are two distinct phases to biomass burning, flaming and smoldering. The phases differ radically from each other in terms of the composition of trace gas emissions and quantity of particulate (smoke) emissions. Ohlemiller (1995) defines smoldering as 'a slow, low temperature form of combustion, sustained by the heat evolved when oxygen directly attacks the surface of a condensed-phase fuel'. Flaming is a higher temperature form of combustion, where an open air flame is fueled by gases released from temperature induced cracking of large chain polymer molecules present in biomass, such as cellulose and lignin (Lobert and Warnatz 1993). The two combustion phases have vastly different character in terms of trace gas and particulate emissions related to the level of fuel oxidation, indexed as combustion efficiency. The flaming phase has high combustion efficiency and smoldering has low combustion efficiency. Summarizing a large number of biomass burning trace gas emission measurements, Koppmann *et al* (2005) report that smoldering fires have higher CO/CO_2, CH_4/CO_2, and VOC/CO_2 ratios. Reid *et al* (2005) found that smoldering fires typically have 3+ times the particulate (smoke) emissions of flaming phase fires per kg of fuel consumed. Thus, distinguishing between flaming and smoldering combustion is critically important for the modeling of atmospheric emissions. In this paper we explore the satellite remote sensing of flaming and smoldering combustion in Indonesia pealands.

Smoldering peat fires in Indonesia are a major source of trace gas and particulate emissions (van der Werf *et al* 2006, 2008, 2010, Tosca *et al* 2011, Hayasaki *et al* 2014). The quantity of peatland burning is

variable from year to year depending on precipitation patterns. Massive peatland fires often occur in El Nino years, when drought conditions set up during the dry season (Siegert *et al* 2001, Gaveau *et al* 2014, Hayasaki *et al* 2014). During these severe fire events, thick smoke palls spread over the entire region, causing hazardous air pollution and closing airports in places like Singapore and Kuala Lumpur (Davies and Unam 1999, Koe *et al* 2001). Peatland burning ranks as one of the difficult environmental issues in Indonesia over concerns for regional air quality, carbon stocks and biodiversity losses (ICCC 2013).

Today's peatland fires in Indonesia are concentrated in areas where the primary forest was logged decades ago (Siegert *et al* 2001, Field *et al* 2009). Drainage ditches installed prior to logging are actively maintained, lowering the water table, particularly during drought events where the upper meter (or more) of the peat dries and is then susceptible to burning. Fires are started for agricultural clearing (Field *et al* 2009, ICCC 2013) and the burning is typically repeated multiple times before the land is planted with a crop, such as oil palm. The objective of the repeated burning is the removal of fallen logs, stumps and root stocks. The dense stock of herbaceous above-ground vegetation is used as the ignition source for the heavier wood elements. Ignition targets the herbaceous vegetation and the recent vegetative growth burns quickly and at a high temperature. This in turn ignites heavier wood remnants, which can burn for many hours, long enough to ignite peat soils, which burn in a smoldering phase. Once smoldering peat fires are established they may continue to burn for extended periods of time, releasing massive quantities of trace gases and smoke (Gaveau *et al* 2014). The surface remains barren and charred for several months, but quickly regains vegetation growth in the next rainy season. If large logs and root stocks remain, the site will be burn again when the opportunity arises.

There is an interplay between flaming and smoldering phase combustion in peatland burning. The initial ignition is achieved with a flaming phase fire, which goes on to ignite smoldering peat fires. Later, the smoldering peat fire can move into areas bearing unburnt above ground biomass, igniting a new round of flaming phase combustion. Fires are spread by a combination of new manmade ignitions, slowly moving smoldering peat burning, and spontaneous ignition of flaming phase fires as the smoldering phase moves into previously unburnt zones.

An ability to generate and update maps distinguish flaming and smoldering fires in would be useful for improving fire management, fire-fighting and emission modeling. Remote sensing is the only practical approach to such mapping given the wide spatial domains across which fires occur. The literature on the remote sensing of smoldering phase combustion is sparse. This may be due to the difficulty in detecting smoldering phase combustion when much of the burning is underground. At certain wavelengths it may be difficult to distinguish flaming and smoldering radiant emissions. One strategy is to distinguish flaming and smoldering fires based on temperature. This is not an option with standard satellite fire products based on detection in a 4 μm channel because temperature is not calculated (Justice *et al* 2002, Giglio *et al* 2003, Schroeder *et al* 2014). Calculating temperature is possible with multispectral fire detections, based on Planck curve fitting (Elvidge *et al* 2013).

Other than temperature, what options exist for discriminating flaming and smoldering phase combustion? Vodacek *et al* (2002) report on a hyperspectral method for detection of flaming phase combustion based on potassium line emissions at 0.766 and 0.700 μm. By implication, hot sources that lack potassium emissions are indicative of smoldering. While this method has not been demonstrated, it may have some merit.

In order to evaluate the discrimination of flaming and smoldering based on temperature, we reviewed available literature on the temperature ranges for the two combustion phases in peatlands. Usup *et al* (2004) collected *in situ* temperatures on smoldering peat fire in Kalimantan, reporting temperatures ranging from 320–550 K. This is half to temperature reported for active fires analyzed with airborne hyperspectral data (Green 1996, Dennison *et al* 2006) and meteorological satellite data (Elvidge *et al* 2013). Peatland fire temperatures in Kalimantan, observed with the BIRD sensor (bi-spectral infra-red detection), ranged from 400–800 K (Siegert *et al* 2004). The lower temperature sources were attributed to peat fires and the higher temperature sources to flaming phase dominated fires.

While the evidence is scant, there is an indication that there is a substantial temperature differential between flaming and smoldering that could potentially be exploited for the identification of smoldering phase peat fires. In this paper we explore active fire features detected in Landsat 8 data collected night in an area of active peat fires present in Riau, Indonesia. There are several favorable characteristics of nighttime Landsat for fire remote sensing research. The pixel footprints (30 m) are small compared to systems such as MODIS and VIIRS, revealing fire fronts and variability inside individual fires. With sunlight eliminated, fires can be unambiguously detected in the short-wave infrared (SWIR) bands centered at 1.6 and 2.2 μm. The long-wave infrared (LWIR) channels are designed to provide land surface temperature data, but have also been used to analyze hot lava (Blackett 2014).

In examining the nighttime Landsat 8 data we found active fire features in both SWIR and LWIR. As expected, active fires are detected in the two SWIR bands (figure 1). In addition, we found that LWIR anomalies are often present in the locations with the SWIR fire detections. Because the SWIR features are unambiguous active fire detections, we concluded that the LWIR anomalies are also active fire features. This

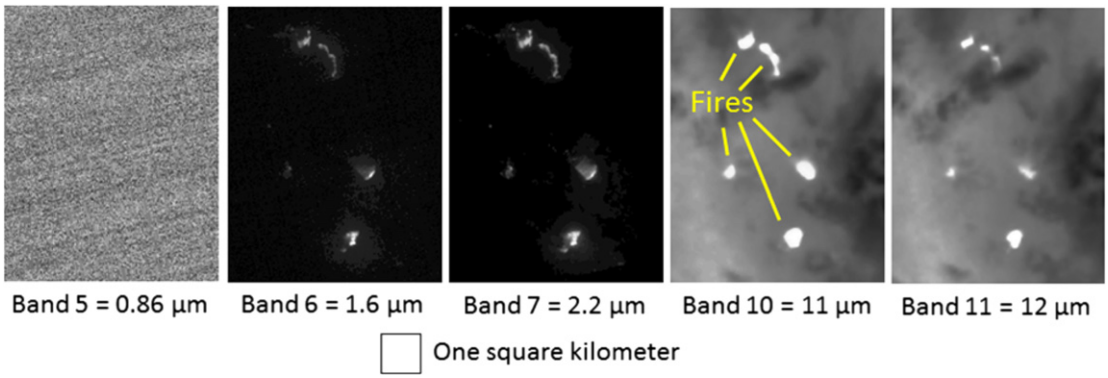

Figure 1. Active fires in four spectral bands in the nighttime Landsat 8 data collected over Riau, Indonesia on 28 March 2014. Detections are found in the SWIR (bands 6 and 7) and LWIR (bnads 10 and 11). Note that active fires are rarely detected in other spectral bands.

raises the question, are the LWIR anomalies associated with flaming or smoldering phase combustion? We investigate this question using five analysis tracks. In the first track, radiant emissions of pixels are modeled using Planck curves for background, flaming and smoldering to identify the best Landsat spectral bands for identification of smoldering radiant emissions. Second, we conduct a specific test to determine if the LWIR radiant emissions can be explained based on flaming phase combustion. Third, we calculate temperature and source sizes for a transect across a paired SWIR and LWIR fire feature. Fourth, we search for active fire features that only appear in one spectral range: SWIR or LWIR. The fifth track is field validation. Finally, we make an estimate of smoldering peat fire detection limits with Landsat 8 data.

2. Planck's law

To explore the source of the LWIR anomalies we rely on Planck's Law, which defines the radiant emission spectrum of objects based on the temperature and emissivity

$$B_\lambda(\lambda, T) = \frac{2hc^2}{\lambda^5}\frac{1}{e^{\frac{hc}{\lambda k_B T}} - 1} \quad (1)$$

where $B\lambda$ = spectral radiance of an object at a particular wavelength

λ = wavelength,

T = degrees Kelvin,

h = the Planck constant.

c = the speed of light,

ϵ = emissivity,

k_B = the Boltzmann constant.

Temperature defines the shape of the curve and the wavelength with peak radiant emissions. Emissivity, which can range from zero to one, defines the amplitude of the curve. In Planck curve fitting, radiances are used to model the Planck curve, generating estimates of the objects temperature and emissivity.

There are two corollaries to Planck's Law that are relevant to fire remote sensing. The Stefan–Boltzmann Law calculates total radiant output (R) based on the temperature and emissivity:

$$R = \epsilon\phi T^4 \quad (2)$$

where ϕ = the Stefen–Boltzmann constant.

The Stefen–Boltzmann Law is an important consideration in the search for smoldering fires. Because of the T^4 term, the radiance spectrum of pixels with multiple temperature components will tend to be dominated by the hottest object present.

Finally, Wien's displacement Law calculates the wavelength of peak radiant emissions based on temperature. As temperature increases, the radiant emission peak shifts to shorter wavelengths. If the temperature of the object is known, this law can be used to calculate the wavelength of peak radiant emissions. Because the flaming phase is about twice as hot as the smoldering phase, Wien's Law indicates the peak radiant emissions for flaming and smoldering will be offset, with flaming phase peaking at shorter wavelengths

$$\lambda_{max} = \frac{b}{T} \quad (3)$$

where b = Wien's displacement constant.

Ordinary Earth objects (land, water, clouds) have temperatures in the range of 260–315 K. The land surface at night in Indonesia has a typical temperature near 300 K, yielding radiant emissions across a range of wavelengths, forming a characteristic 'Planck curve' for a blackbody, with a peak at 9.66 μm. Blackbodies are objects that radiate efficiently at all wavelengths, rated with an emissivity = 1.0. Clouds, water and vegetation radiate very nearly as blackbodies. Some rocks

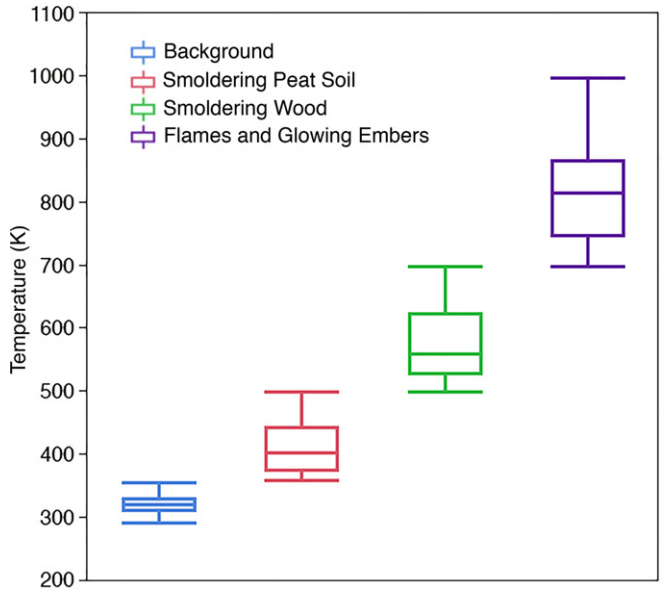

Figure 2. Box chart showing the temperature distribution of four types of surfaces: background, smoldering peat soil, smoldering wood, flames and glowing embers.

Table 1. Landsat 8 spectral bands and spatial resolutions.

Band designation	Bandpass (μm)	Spatialresolution (meters)
Band 1—blue	0.43–0.45	30
Band 2—blue	0.45–0.51	30
Band 3—green	0.53–0.59	30
Band 4—red	0.64–0.67	30
Band 5—NIR	0.85–0.88	30
Band 6—SWIR	1.57–1.67	30
Band 7—SWIR	2.11–2.29	30
Band 8—panchromatic	0.50–0.68	15
Band 9—NIR	1.36–1.38	30
Band 10—LWIR	10.60–11.19	100 resampled to 30
Band 11—LWIR	11.50–12.51	100 resampled to 30

and soils have minor departures from blackbody behavior. Objects with uniformly lower radiant emissions than blackbodies are referred to as 'graybodies'. Sub-pixel hot sources appear as graybodies in satellite remote sensing. This concept is incorporated in Planck's Law as the emissivity term. Elvidge *et al* (2013) introduced the term 'emission scaling factor' (esf) as a replacement for the term 'emissivity' for sub-pixel hot sources. The use of esf instead of emissivity is to distinguish sub-pixel graybodies from graybodies arising from molecular level inefficiencies in radiant capabilities.

3. Data collection

The study uses two primary types of data: nighttime Landsat and surface temperature data collected on transects crossing active fire areas in Kalimantan. Daytime Landsat data of Indonesia are collected on routine basis, so there is no need to schedule collections. In contrast, nighttime Landsat collections are non-routine and must be scheduled through the USGS collection manager. In this study we use Landsat 8 data collected on Riau, Sumatra (Path 2, Row 185) on 28 March 2014. Riau was the site of extensive peat fires in February and March of 2014, with massive smoke production. Data were collected in all eleven available spectral bands (table 1).

Infrared temperature data of background and active fires were measured at a variety of sites surrounding Palangkaraya, Central Kalimantan in September 2014. The measurements were collected using a CEM Instruments DT-9862 Professional Infrared Video Thermometer, which has a dynamic range spanning 215–2373 K. The instrument operator can aim the unit to collect temperature data on specific objects based on a pair of red laser field-of-view guides. Data were collected along transects across vegetated peatlands, recently burn peatlands, and areas of active fires. The instrument collect video frames during temperature collection. The frames are stamped with date, time and temperature for future reference. In addition, the operator collected field notes indicating the types of surfaces being measured.

4. Analysis and results

4.1. Temperature ranges for flaming and smoldering

Figure 2 shows a histogram of the field temperature data collected in September 2014 in areas surrounding Palangkaraya, Central Kalimantan. A total of 9139 temperature records were collected. Field notes and video frame images were used to divide the data into

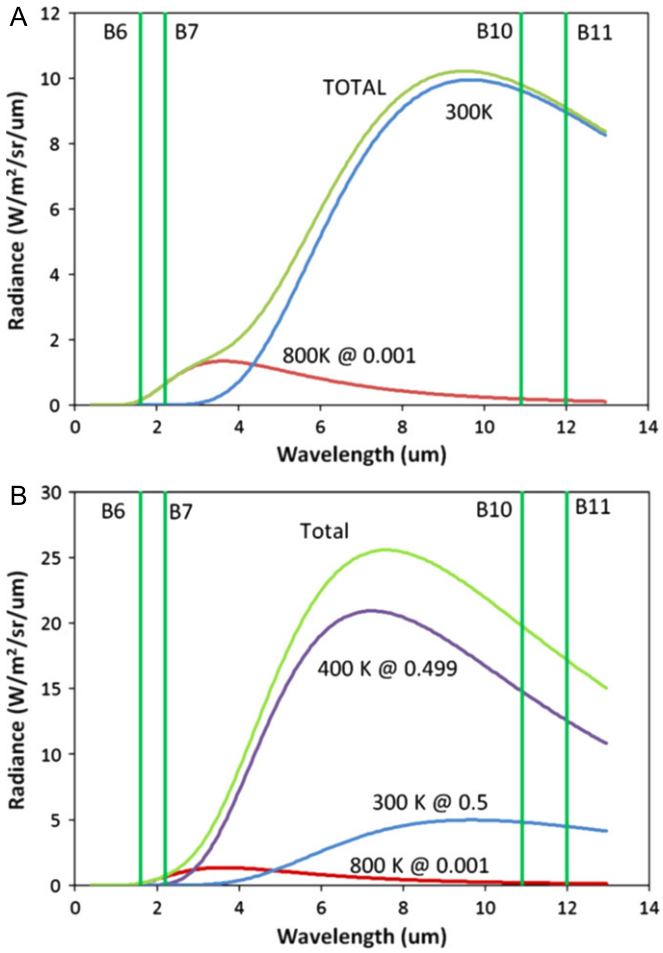

Figure 3. (A) Mixture modeling of a Landsat 8 pixel containing a 300 K background and an 800 K subpixel flaming phase fire covering 1/1000 of the surface. (B) Mixture modeling of a Landsat 8 pixel with half of the surface at 300 K (background), nearly half smoldering at 400 K, and an 800 K flaming phase fire covering 1/1000 of the surface.

three sets: background, smoldering, and flaming. The large spike at the low end of the temperature scale is the background, with temperatures ranging from 290–360 K, with an average of 322 K. The background is quite warm because of solar heating of the low albedo peat surfaces. The smoldering peat soil areas had temperatures in the range of 360–500 K with an average temperature of 412 K. This is comparable to the 320–550 K range than that published by Usup *et al* (2004). Smoldering wood in close proximity to flaming had temperatures ranging from 500–700 K. Open flames and glowing embers had temperatures ranging from 700–1000 K and an average of 813 K.

4.2. Modeling the radiant emissions of flaming and smoldering

By modeling the radiant emissions of flaming and smoldering it will be possible to identify the promising spectral ranges for distinguish flaming from smoldering. For the modeling we will use a typical temperature for flaming, smoldering, and background and set source sizes based on field observations. In the field we saw the smoldering phase was spatially extensive and in some cases could fill an entire Landsat pixel. In contrast, the flaming phase was typically quite small, on the order of square meters. The modeling is done with software that generates Planck curves based on temperature and the proportion of the field of view occupied by the source.

Using Planck's Law, radiant emission models were developed for two hypothetical nighttime Landsat pixels. The first has a 300 K background and an 800 K flaming phase fire covering 1/1000 of the surface. The Planck curve mixture model (figure 3(A)) has two radiant emission components: (1) an emission spectrum from the 300 K background with peak radiant emissions at 9.66 μm and total radiant power of 459 W m^{-2}, and (2) a flaming phase emission spectrum, with lower radiant output (23.2 W m^{-2}) than the background and peak radiant emissions at 3.62 μm. With zero solar radiance, the presence of the flaming phase can be confirmed based on radiance detected in the SWIR bands 6 and 7. The background has no detectable radiance in the SWIR.

The second pixel has three components: half of the surface is at the background temperature of 300 K, nearly half (0.499) of the surface is smoldering at

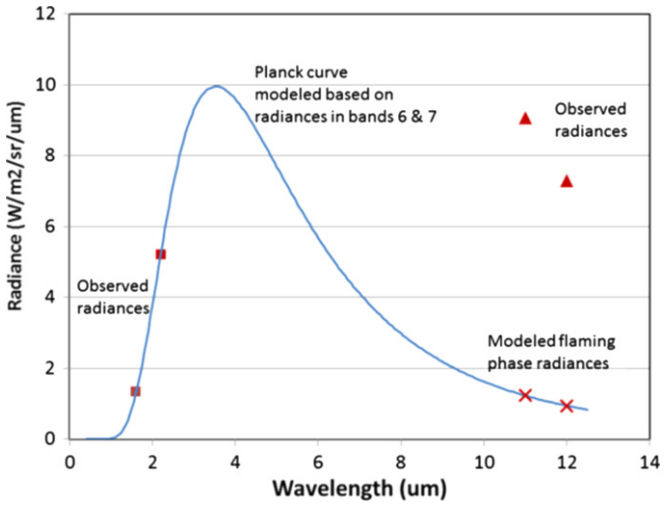

Figure 4. The flaming phase radiances in the LWIR can be modeled with the two SWIR band radiances via Planck curve fitting. The fitting indicates the flaming phase temperature is 825 K. The radiances in bands 10 and 12 are comparable to the radiance in band 6.

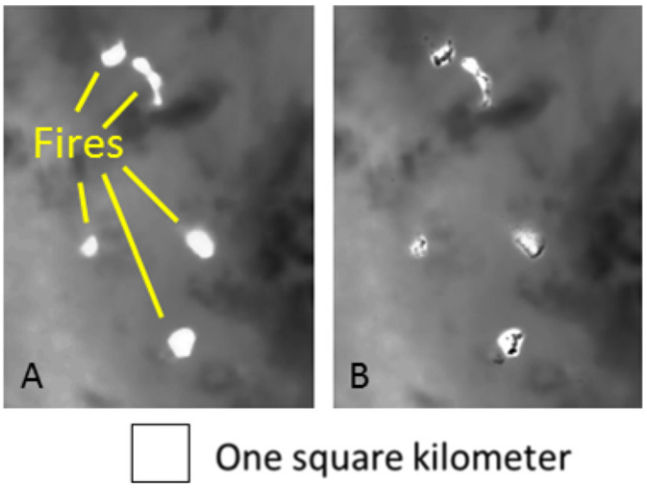

Figure 5. (A) Original band 10 data. (B) Band 10 radiance minus the flaming phase band 10 radiance. The persistence of the LWIR features confirms the presence of smolder phase combustion. Dark spots are induced near the centers of the active fire features, at the peak of band 10 radiance.

400 K, and 0.001 of the surface has flaming phase at 800 K (figure 3(B)). Here the Planck curve from the smoldering phase has far higher radiant output (725 W m^{-2}) than the background and peak radiant emissions at 7.24 μm. The presence of the smoldering component enhances the radiances in band 10 by 3X and band 11 by 2.8X. The flaming phase radiance represents less than 1% of the total radiance in bands 10 and 11.

There is a ~400 K temperature differential between flaming and smoldering. The flaming phase Planck curve is shifted to shorter wavelengths as compared to the smoldering phase. Based on the radiant emission mixture modeling, the SWIR is a good place to detect the flaming phase. The Landsat SWIR bands fall on the leading edge of the flaming phase radiant emissions, out of range from radiant emissions from the background and largely clear of radiant emissions from the smoldering phase. The smoldering phase has peak radiant emissions in the 7 μm region, where the atmosphere is opaque due to strong absorptions by water vapor. This leaves the LWIR as the best place to detect smoldering combustion. The Landsat bands 10 and 11 miss the peak radiant emissions from smoldering, but smoldering will produce strong radiant emissions in these spectral bands, creating thermal anomalies relative to the background.

4.3. Test for confirming smoldering phase detection in the LWIR

A test was designed for confirming whether the LWIR active fire features are associated with flaming or smoldering phase burning. The Planck curve mixture modeling suggests that the temperature differential between flaming and smoldering is substantial enough

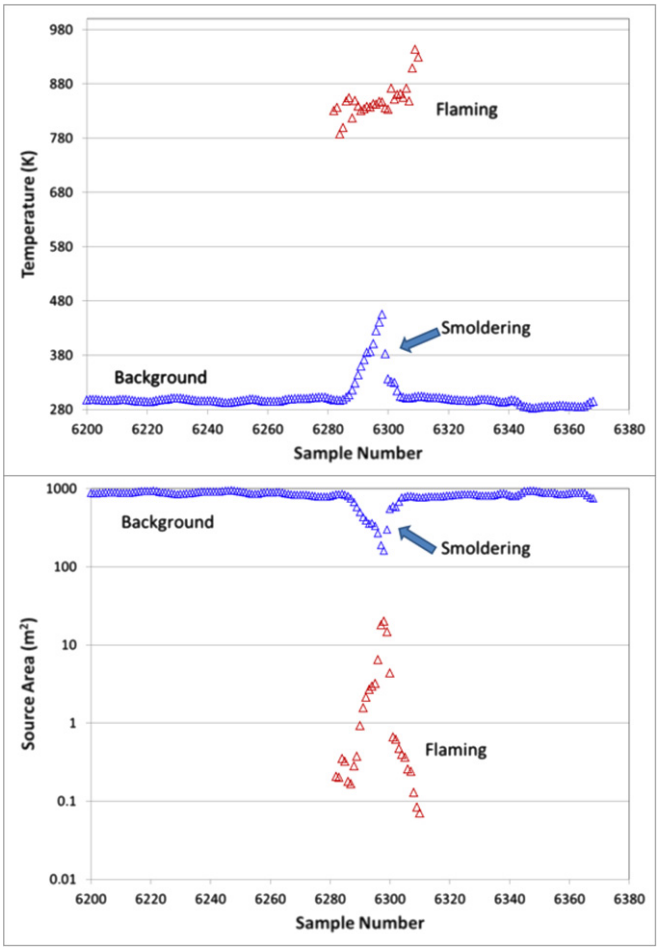

Figure 6. SWIR and LWIR temperatures and source areas calculated via Planck curve fits. The red points are from the SWIR and blow points are from the LWIR.

to induce a measure of separability of the combustion phases using the Landsat spectral bands. That is to say, the radiances observed in the SWIR bands sample the leading edge of the flaming phase Planck curve, while radiant emissions from the smoldering phase are concentrated at longer wavelengths. The LWIR bands record radiances from the trailing edge of smoldering combustion, plus emissions from background. To test the origin of the LWIR active fire anomalies, we can subtract the flaming phase radiance in band 10 and see if the features persist. If the LWIR fire anomalies persist after subtraction of the flaming phase radiance it proves the anomalies are coming from smoldering phase combustion.

The first processing step is to fit flaming phase Planck curves with the two SWIR bands, yielding flaming phase radiances in the LWIR bands (figure 4). The Planck curve fitting is done with the Simplex method described in Elvidge *et al* (2013). In the second step, the flaming phase radiances are subtracted from the observed LWIR radiances. The results for band 10 are shown in figure 5. We found that thermal anomalies persist after subtracting the flaming phase radiances. This confirms the presence of smoldering peat fires. However, dark pixel sets are introduced into the thermal band residuals in the areas with the larger flaming phase source areas.

We were able to replicate the dark spots using Planck curve fitting applied to pixel mixture model as outlined in section 4.2. By stepping up the smoldering source area, smoldering radiances increased in band 7. This skews the flaming phase Planck curve fitting results with reduced temperatures, increased source sizes and higher LWIR radiances. This indicates that when the smoldering phase occupies a large proportion of the pixel footprint, the assumption that the SWIR is free of significant smoldering phase radiance breaks down.

4.4. SWIR versus LWIR planck curve fitting

Another method for testing the hypothesis that the Landsat 8 fire pixels contain two combustion phases is to apply separate Planck curve fitting to the SWIR and LWIR. If the two spectral ranges yield similar Planck curves, their temperatures and source sizes will be very similar, indicating that only one combustion phase is present, with detection in both SWIR and LWIR.

To implement this test a single line of data from the image shown in figure 1 is analyzed. An atmospheric correction is applied to the radiances. Then

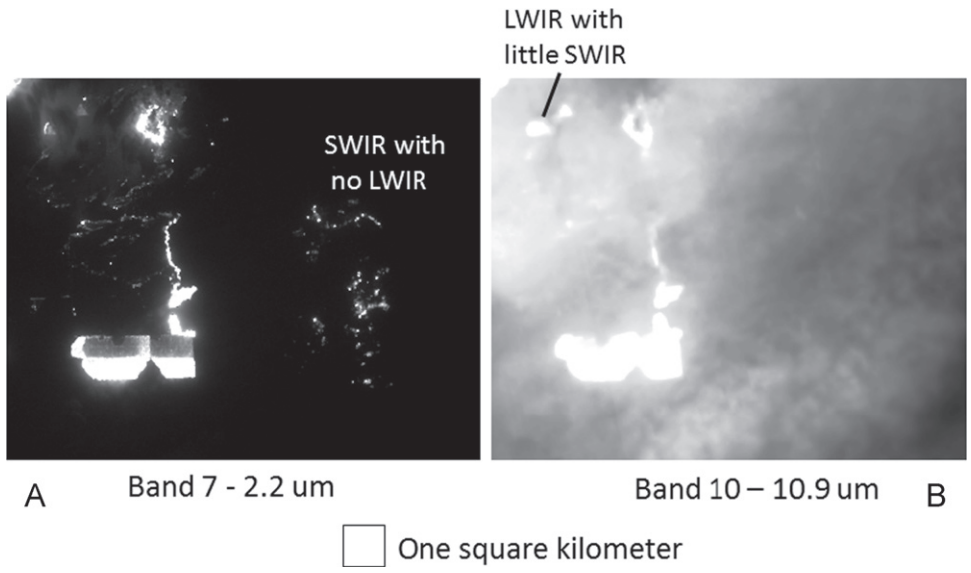

Figure 7. In most cases the LWIR and SWIR active fire features are co-located. But it is possible to find SWIR detections that lack LWIR thermal anomalies. This is an indication of flaming phase fires that have not initiated smoldering. (A) Band 7 image showing areas with active fires that are not present in the LWIR. (B) Band 10 image showing active fires that are faintly expressed in the SWIR.

Figure 8. Field photo collected from the edge of the field validation site visited on 28 August 2014, five months after the LWIR active fire anomaly was observed in nighttime Landsat 8 data. The site is bounded on one side by a drainage ditch, in the foreground of the photo. The site has thick peat soil and a sparse quantity of fresh vegetation regrowth. In the center of the photo there is a charred tree trunk remnant.

two separate Planck curves are fit to the radiances, one for the two SWIR bands and the other for the two LWIR bands. The SWIR fitting was only done for pixels with a detectable signal in band 6 to avoid spurious results from the sensor dark current. Temperature and source area are derived through a simplex fitting process (Lagarias *et al* 1998). The results in figure 6 indicate that there are two distinct active fire phases present along the transect: flaming and smoldering.

The SWIR radiances produced an average temperature of 850 K and an average source area of 2.8 m. Both the temperature and source area match expectations for flaming phase. The background has an average temperature of 297 K and average source size of 878 m^2, consistent with a full Landsat pixel (900 m^2). In the active fire area, the LWIR temperature rises to 455, with an average of 365 K. As the temperature rises, source area declines, reaching a minimum of 160 m^2. The LWIR temperature results are consistent with smoldering combustion mixing with background. Note that the LWIR temperature and source size estimates presented in figure 6 are flawed by spectral mixing of smoldering and background.

4.5. Identification of SWIR only detections

In most case the LWIR anomalies are collocated with SWIR detection features, indicating that the two combustion phases are typically present together in single Landsat pixels. A search was conducted to find examples of active fires that have either SWIR only or LWIR only. It is possible to find example of SWIR only

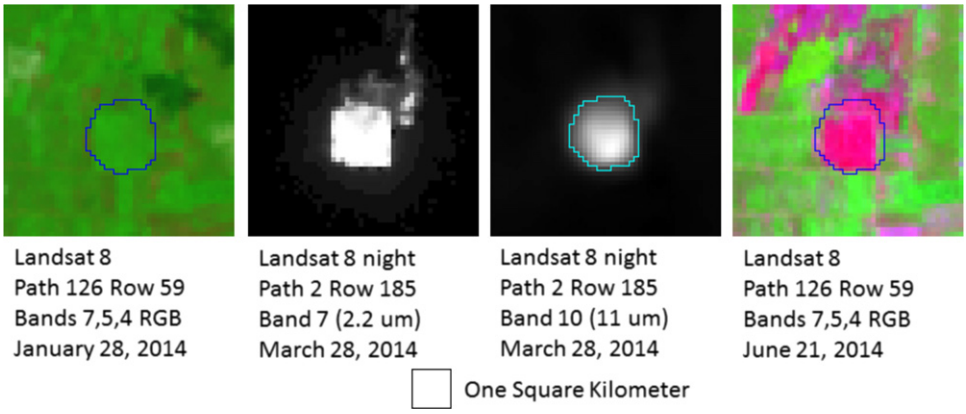

Figure 9. This site was visited on 28 August 2014, five months after the LWIR fire anomaly was observed in nighttime Landsat 8 data. The outline of the LWIR fire anomaly is drawn as a vector. In late January, 2014 the area was covered by green vegetation. In June the area had the spectral signature of a burn scar.

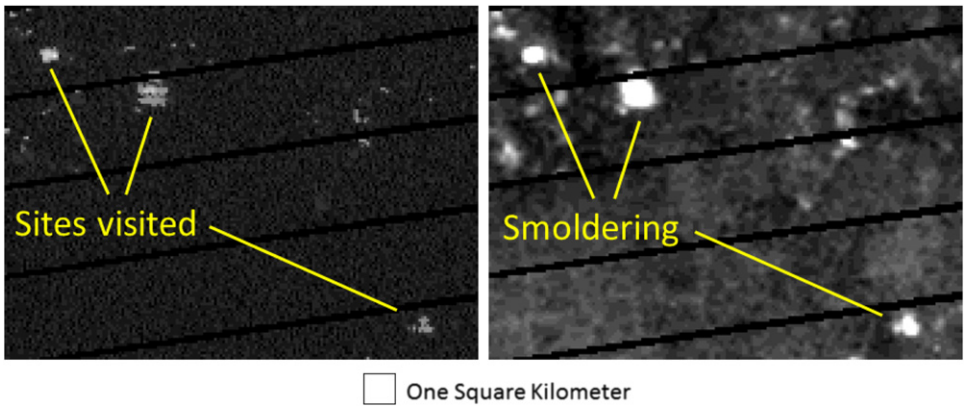

Figure 10. Nighttime Landsat 7 data collected on 20 September 2014 of Path 227, Row 182. The image on the left is SWIR (2.2 μm). The LWIR anomalies are pronounced. The three sites indicated were visited in the field on 21 September, confirming the presence of smoldering peat fires.

Figure 11. Field photo collected 21 September 2014 at a LWIR fire anomaly site imaged by Landsat 7 the previous night. The site was still smoldering, as confirmed by thermal radiometer data and the presence of smoke emitting from surfaces with no flames present.

active fires (figure 7(A)), indicating the presence of flaming phase, but no detectable smoldering phase. It is also possible to find examples of LWIR active fire detection with reduced levels of SWIR (figure 7(B)), but no example could be found of LWIR detection in complete absence of SWIR signal.

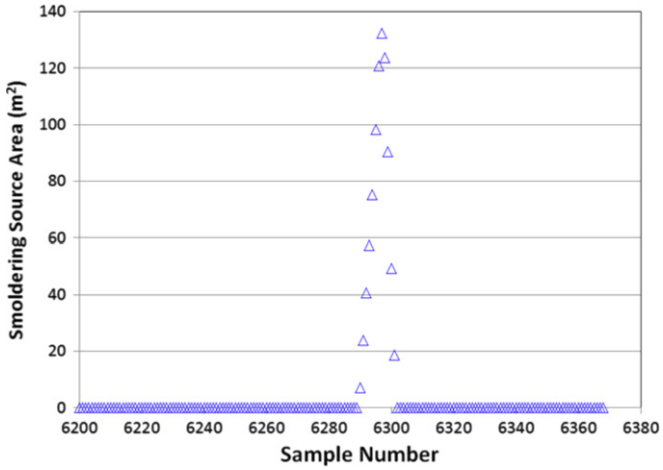

Figure 12. Smoldering source area for pixels along the figure 6 transect. The source area was calculated assuming a background temperature of 300 K and smoldering temperature of 400 K.

5. Field validation

Four of the LWIR fire anomalies were visited in the field to confirm the presence of smoldering peat fires. The first site to be visited is from the 28 March 2013 Landsat 8 scene used in the testing reporting in the above section. The specific location is 0.949 N, 102.131 E. The site was visited five months after the nighttime Landsat data collection, on 28 August 2014 (figure 8). There was a small quantity of fresh vegetation growth present, typical for sites with recent burning. Overall, the site had characteristics consistent with recent peat fire burning. The soil was clearly peat. Indications of recent peat burning included a sparse set of fresh regrowth, charred tree trunks and deep holes burnt into areas surrounding tree root stands. An examination of daytime Landsat acquired before and after the 28 March fire observation indicate that early in 2014 the plot was covered by green vegetation and in June it was burn scar (figure 9).

To collect more timely validation data, a field survey team went to Kalimantan in September 2014. Three actively smoldering LWIR fire anomalies were validated on 21 September 2014, less than 24 h after detection by Landsat 7 collected at night on Path 227 Row 182 (figure 10). Thermal radiometer measurements confirmed the presence of smoldering combustion at all three sites. Smoke was emanating from the soils (figure 11), an additional confirmation of smoldering.

6. Detection limits for smoldering peat fires

To estimate the detection limits for smoldering peat fires, a spectral mixture model was developed for the transect shown in figure 6. The model was constrained by the atmospherically corrected radiances in bands 10 and 11, plus fixed temperatures for background and smoldering. The background temperature was set to 300 K and the smoldering to 400 K. A simplex process was used to fit esf values for each pixel to match the radainces. The esf values were then multiplied by 900 m^2 to estimate the area of active smoldering present in the pixel. The results are shown in figure 12, with active smoldering surface areas ranging from 7 to 132 m^2. To estimate the detection limit we take values from the third pixels in from the edge to avoid background contaminaion associated with the resampling of the original 100 m pixels to 30 m. This yields detection limit estimates in the 40–90 m^2 range. This coincides with subpixel areas of 4–10% of the pixel surface.

7. Conclusion

Smoldering peat fires can be distinguished from flaming phase combustion based on temperature. The temperature of smoldering peat fires is in the range of 60–500 K approximately half the temperature of flaming phase combustion. We explored the possibility that this temperature differential can be exploited to make separate identification of flaming and smoldering phase combustion in Indonesia peatlands using nighttime Landsat 8 data. We found active fire features in four spectral bands: two SWIR bands and two LWIR bands. The combustion phase source for the LWIR active fire features was investigated with five methods: pixel modeling, flaming phase subtraction, temperature calculations based on Planck curve fitting of SWIR versus LWIR, identification of SWIR active fire features that lack LWIR anomalies, and field validation. All five lines of investigation point to smoldering combustion as the source for the LWIR fire anomalies.

Peatland fires often have flaming and smoldering combustion phases present simultaneously within pixel footprints. Traditional fire remote sensing algorithms based on the 4 μm region are skewed towards the detection of flaming phase fires, which have peak

radiant emissions in the 3–4 μm mid-wave infrared region. Smoldering combustion has peak radiant emission in the 7 μm region, a spectral range dominated by atmospheric water absorption. While it is not possible to see to the ground at 7 μm, LWIR remote sensing is possible in the 8–12 μm region. Mixed pixel modeling for flaming, smoldering and background point to the LWIR is the best spectral range for observing the radiant emissions from smoldering phase combustion with minimal interference from flaming phase radiant emissions.

To test the hypothesis that the LWIR active fire feature are associated with smoldering phase combustion we modeled and subtracted the flaming phase radiance. Planck curve fitting using radiances from the two SWIR bands provided estimates of the flaming phase radiance in the LWIR. This was then subtracted from the LWIR radiance. The persistence of the active fire features after the subtraction indicates the LWIR active fire features can be attributed to the presence of smoldering phase combustion.

Separate Planck curve fitting of the SWIR versus LWIR yielded vast different temperatures, indicating the presence of flaming and smoldering combustion phases. Temperatures from the two SWIR band radiances average 850 K, typical of flaming phase combustion. The peak temperature from the LWIR fitting was 455, in the range of smoldering based on published reports (Usup *et al* 2004) and field data collected by the authors.

In most cases, SWIR and LWIR active fire features are co-located. However, if the SWIR and LWIR active fire features correspond to flaming and smoldering, then there should be cases where only SWIR or LWIR are present in isolation. We looked for examples of this and it is relatively easy to find SWIR active fire features that lack LWIR anomalies. This is an indication of flaming phase combustion that has not yet ignited smoldering. We found cases where the LWIR active fire features had diminutive SWIR features, but no cases where LWIR active fire features are devoid of SWIR signal.

There is evidence to indicate that the calculation of flaming and smoldering temperatures and source sizes would benefit from methods that account for spectral mixing occurring between flaming, smoldering and background. One indication of this is the pixel darkening in the centers of LWIR active fire features when the flaming phase radiance is subtracted. We were able to duplicate this effect by stepping the pixel mixture modeling in Section 4.2 to high levels smoldering spatial coverage. Another indication is the temperature and source area ramps found marking the transition from background to smoldering in figure 6. Temperatures ramped up moving toward the peak band 10 radiance, while source areas declined. This suggest that the LWIR active fire feature contains a mixture of smoldering and background that propagates into the Planck curve fitting. The third indication is the fact that all of the LWIR active fire features had some level of SWIR fire detection. It may be possible to backout these phase interactions to reduce errors in the calculation of temperature and source areas for flaming and smoldering. This is a topic for future research.

The advantage of nighttime Landsat in our study is that it was possible to make unambiguous detection of active fires in two SWIR bands and to attribute the full radiance to combustion. However, the basic features can also be observed in daytime Landsat-8 bands 7, 10, and 11. This is an important consideration, since nighttime Landsat data are not routinely collected. It may be possible to reconstruct a history of flaming and smoldering events in Indonesia through mining of the Landsat archive. Detection limits for smoldering peat fires in nighttime Landsat 8 data are in the range of 40–90 m^2.

The results indicate that the SWIR and LWIR spectral data can be used to map and monitor flaming and smoldering phase combustion. This could be used to improve fire management and emission modeling for the peatland fires in Indonesia and elsewhere. There are other remote sensing sources where this capability may be developed. The authors are currently studying flaming versus smoldering combustion with VIIRS data. In addition to Landsat, other satellite systems, such as Digital Globe's Worldview 3 could be quite effective at discriminating flaming and smoldering combustion. Another avenue to consider is airborne sensing systems that could fly under the clouds collecting SWIR and LWIR spectral data. We fully expect that each of these avenues will be investigated by entities interested to improve fire management and emission modeling.

Acknowledgments

This research was funded by the US Forest Service, International Program. The paper benefited from points raised by the reviewers.

References

Blackett M 2014 Early analysis of Landsat-8 thermal infrared sensor imagery of volcanic activity *Remote Sens.* **6** 2282–95

Davies S J and Unam L 1999 Smoke-haze from the 1997 Indonesian firest fires: effects on pollution levels, local climate, atmospheric CO_2 concentrations, and tree photosynthesis *Forest Ecology Manage.* **124** 137–44

Dennison P E, Charoensiri K, Roberts D A, Peterson S H and Green R O 2006 Wildfire temperature and land cover modeling using hyperspectral data *Remote Sens. Environ.* **100** 212–22

Elvidge C D, Zhizhin M, Hsu F C and Baugh K E 2013 VIIRS nightfire: satellite pyrometry at night *Remote Sens.* **5** 4423–49

Field R D, van der Werf G R and Shen S S P 2009 Human amplification of drought-induced biomass burning in Indonesia since 1960 *Nat. Geosci.* **2** 185–8

Gaveau D L A *et al* 2014 Major atmospheric emissions from peat fires in Southeast Asia during non-drought years: evidence from the 2013 sumatran fires *Sci. Rep.* **4** 1–6

Giglio L, Descloitres J, Justice C O and Kaufman Y J 2003 An enhanced contextual fire detection algorithm for MODIS *Remote Sens. Environ.* **87** 273–82

Green R O 1996 Estimation of biomass fire temperature and areal extent from calibrated AVIRIS spectra *Summaries of the 6th Annual JPL Airborne Earth Science Workshop* vol 1 (Pasadena, CA: Jet Propulsion Laboratory, JPL Publication 96-4) pp 105–13

Hayasaki H, Noguchi I, Rutra I E, Yulianti N and Vadrevu K 2014 Peat-fire-related air pollution in Central Kalimantan, Indonesia *Environ. Pollut.* **195** 257–66

ICCC 2013 *International Indonesia Peatland Conservation 2013 Synthesis Report* Indonesia Climate Change Center, Jakarta, Indonesia (http://iccc-network.net/document/20130613_iipc2013_synthesis.pdf)

Justice C O, Giglio L, Korontzi S, Owens J, Morisette J T and Roy D 2002 The MODIS fire products *Remote Sens. Environ.* **83** 244–62

Koe L C C, Arellano A F Jr and McGregor J L 2001 Investigating the haze transport from 1997 biomass burning in Southeast Asia: its impact upon Singapore *Atmos. Environ.* **35** 2723–34

Koppmann R, von Czapiewski K and Reid J S 2005 A review of biomass burning emissions, part I: gaseous emissions of carbon monoxide, methane, volatile organic compounds, and nitrogen containing compounds *Atmos. Chem. Phys. Discuss.* **5** 10455–516

Lagarias J C, Reeds J A, Wright M H and Wright P E 1998 Convergence properties of the Nelder–Mead simplex method in low dimensions *SIAM J. Optim.* **9** 112–47

Lobert J M and Warnatz J 1993 Emissions from the combustion process in vegetation *Fire in the Environment: The Ecological, Atmospheric, and Climatic Importance of Vegetation Fires* ed P J Crutzen and J G Goldhammer (New York: Wiley)

Ohlemiller T J 1995 Smoldering combustion *SFPE Handbook of Fire Protection Engineering* ed M A Quincy, P J DiNenno, C L Beyler, R L P Custer and W D Walton, 2nd edn (Quincy, MA: National Fire Protection Association) section 2, chapter 11, pp 171–9

Reid J S, Koppmann R, Eck T F and Eleuterio D P 2005 A review of biomass burning emissions part: II. Intensive physical properties of biomass burning particles *Atmos. Chem. Phys.* **5** 799–825

Schroeder W, Oliva P, Giglio L and Csiszar I A 2014 The new VIIRS 375 m active fire detection data product: algorithm description and initial assessment *Remote Sens. Environ.* **143** 85–96

Siegert F, Ruecker G, Hinrichs A and Hoffmann A A 2001 Increased damage from fires in logged forsts during droughts caused by El nino *Nature* **414** 437–40

Siegert F, Zhukov B, Oertel D, Limin S, Page S E and Rieley J O 2004 Peat fires detected by the BIRD satellite *Int. J. Remote Sens.* **25** 3221–30

Tosca M G, Randerson J T, Zender C S, Nelson D L, Diner D J and Logan J A 2011 Dynamics of fire plumes and smoke clouds associated with peat and deforestation fires in Indonesia *J. Geophys. Res.—Atmos.* **116** 1–14

Usup A, Hashimoto Y, Takahashi H and Hayasaki H 2004 Combustion and thermal characteristics of peat fires in tropical peatland in Central Kalimantan, Indonesia *Tropics* **14** 1–19

van der Werf G R, Dempewolf J, Trigg S N, Randerson J T, Kasibhatla P S and Giglio L 2008 Climate regulation of fire emissions and deforestation in equatorial Asia *Proc. Natl Acad. Sci. USA* **105** 20350–5

van der Werf G R, Randerson J T, Giglio L, Collatz G J, Kasibhatla P S and Arellano A F 2006 Interannual variability in global biomass burning emissions from 1997 to 2004 *Atmos. Chem. Phys.* **6** 3423–41

van der Werf G R, Randerson J T, Giglio L, Collatz G J, Mu M and Kasibhatla P S 2010 Global fire emissions and the contribution of deforestation, savanna, forest, agricultural, and peat fires (1997–2009) *Atmos. Chem. Phys.* **10** 11707–35

Vodacek A, Kremens R L, Fordham A J, Vangorden S C, Luisi D, Schott J R and Latham D J 2002 Remote optical detection of biomass burning using a potassium emission signature *Int. J. Remote Sens.* **23** 2721–6